Error Reduction of 2DOF Gimbal Gyros Using LQG/LTR Controller

H.Torab[1], M. Farrokhi[1,2]
[1] *Department of Electrical Engineering*
[2] *Center of Excellence for Power System Automation and Operation*
Iran University of Science and Technology
Tehran 16486 - IRAN
htorab@ee.iust.ac.ir, farrokhi@iust.ac.ir

Abstract—In this paper, the dynamic equations and error reduction of 2DOF gimbal gyros are investigated. One of the major error sources in such gyros is the gimbal lock, which causes major errors and losing one degree of freedom. This error source is eliminated in this paper using a permanent magnet motor as the torquer. Moreover, using an LQG/LTR controller will guarantee the closed-loop system stability. In addition, effects of other error sources such as the drift, the measurement noise and the nutation are eliminated or reduced. Using the proposed method, one can easily measure the output angular rates using multiplication of the measured input voltage of the torquer and the system scale factor.

Key Words: 2DOF gimbal gyro, gyroscope feedback control, LQG/LTR control, gimbal lock, INS

1. INTRODUCTION

Inertial sensors such as gyroscopes are important parts of Inertial Navigation Systems (INS) that measure vehicle angular rate or deflection angle. Therefore, even a slight error in gyro outputs could lead to serious errors and malfunction of the system and results in severe system performance degradation. Hence, it is very important to detect and remove the faults effects in gyros.

Mechanical gyros are the first and very important types of gyros, which have many applications with their various types. There are two important types of mechanical gyro: 1) rate gyros and 2) displacement or free gyros, which measure the angular rate and the deflection angle of the vehicle, respectively. These gyros exist in single and two Degree-of-Freedom. The most important type of the mechanical gyros is the Dynamically Tuned Gyro (DTG) and gimbal gyro. Gimbal gyros could be used as the rate gyro or the free gyro; DTGs are usually used as the free gyro to measure the deflection angle.

Single DOF (SDOF) gyros have been widely studied in the literatures. Although various algorithms have been developed to investigate the faults in gyros and INS, few results dealt with specific faults and sometimes the faults are left undefined or are only handled based on very simplified assumptions. In [1] a robust Kalman filter is applied to eliminate some faults. However, the fault characteristics are not described from an engineering point of view. In [2] and [3] the gyro failures are classified as the hard and soft failures. The hard failures are modeled by zeroing out the corresponding rows in the measurement matrix while the soft failures are simulated by either adding biases or increasing the variance of the noise at the gyro outputs. Zhang and Jiang [4] have adopted a similar formulation for hard gyro failures in their investigation of fault-tolerant control systems; later they continue their research on analysis of various faults sources in rate gyros [5].

Due to the fact that there is no noticeable research on 2DOF mechanical gyroscopes, this remains already an open problem in the control and INS literatures. In this paper, dynamic equations and error reduction of such gyros are investigated. By designing a suitable controller and using a permanent magnet motor as the torquer, the effects of the bias and drift errors and measurement noise are reduced. The advantages of this methodology are eliminating the gimbal lock phenomenon and disturbances, and reducing the effect of other common faults such as nutation and noises. The gimbal lock is a major error source, which occur in 2DOF gyros and can cause loosing one degree of freedom. In this way, the measured angular rates are obtained form the product of the measured torquer input voltage and the system scale factor.

In this paper, an LQG/LTR controller, which involves a Kalman filter and an LQR controller, is used to guarantee the stability of the closed-loop system and reduce the effects of disturbances and measurement noises. One of the main advantages of the proposed method is that it can be easily implemented.

This paper is organized as follows. Section 2 shows how to obtain nonlinear equations of the 2DOF gimbal gyro, followed by linearization about the zero equilibrium point, which provides linear state-space equations of the gyroscope. In Section 3, the control structure and the system scale factor is investigated. Section 4 defines important error resources of gyroscope. Section 5 provides simulation results of the closed-loop system, where failures are also considered. Section 6 concludes the paper.

Notations: The following notations are used in this paper:

(X, Y, Z): inertial coordinate axis
(x, y, z): moving (body) coordinate axis
ω_s: speed of spinning
ω: angular velocity of gyroscope
Ω: angular velocity of vehicle
$\dot{\omega}$: angular acceleration

I : inertial momentum
H : angular momentum of rotor
D : damping coefficient
C : spring constant
T : torque about output axis
θ : gimbal deflection

2. Model of 2DOF Free Gyroscopes

Gyros measure the roll, yaw, and pitch angles of a vehicle. Figs. 1 and 2 show the common configuration of a gimbal gyro, including a 2DOF gyro, springs, which restrain the gimbals from precessing, dampers that damp out oscillations, and pickoffs that generate electrical output signal proportional to the angle of gimbals from the zero position.

Mathematical Model of a 2DOF Gimbal Gyro

To obtain the gyro dynamic equations, first consider the way one can bring gimbals to the final position (Fig. 3). This action consists of θ_x degrees of rotation about the *X*-axis followed by θ_y degrees of rotation about the *Y*-axis.

It is assumed here that ω_s has a negligible change, inertial momentum of gimbals x and y are equal ($I_x = I_y = I$), and gimbals can rotate freely. There is also a torquer for each gimbal that causes gimbals to rotate only less than ± 1 degree. Hence,

$$\begin{cases} \cos\theta \cong 1 \\ \sin\theta \cong \theta \end{cases} \tag{1}$$

The angular rate of the gyro and the vehicle about the inertial coordinate axis are

$$\vec{\omega} = \vec{\omega}_x + \vec{\omega}_y + \vec{\omega}_z + \vec{\omega}_s \tag{2}$$

$$\vec{\Omega} = \vec{\omega}_x + \vec{\omega}_y + \vec{\omega}_z \tag{3}$$

Referring to Fig. 3, ω and $\dot{\omega}$ can be found as

$$\begin{cases} \omega_x = \dot{\theta}_x \cos\theta_y \\ \omega_y = \dot{\theta}_y \\ \omega_z = \omega_s + \dot{\theta}_x \sin\theta_y \end{cases} \tag{4}$$

$$\begin{cases} \dot{\omega}_x = \ddot{\theta}_x \cos\theta_y - \dot{\theta}_x\dot{\theta}_y \sin\theta_y \\ \dot{\omega}_y = \ddot{\theta}_y \\ \dot{\omega}_z = \dot{\omega}_s + \ddot{\theta}_x \sin\theta_y + \dot{\theta}_x\dot{\theta}_y \cos\theta_y \end{cases} \tag{5}$$

Replacing (4) and (5) in Euler equation and simplifying yields the dynamic equations of the gyro as [6]

$$\begin{cases} T_x = I_x\dot{\omega}_x + \Omega_y I_z\omega_z - \Omega_z I_y\omega_y \\ T_y = I_y\dot{\omega}_y + \Omega_z I_x\omega_x - \Omega_x I_z\omega_z \end{cases} \tag{6}$$

$$\begin{cases} T_x = I\ddot{\theta}_x + (I_z - 2I)\dot{\theta}_x\dot{\theta}_y\theta_y + H\dot{\theta}_y + D_x\dot{\theta}_x + C_x\theta_x \\ T_y = I\ddot{\theta}_y + (I - I_z)\dot{\theta}_x^2\theta_y - H\dot{\theta}_x + D_y\dot{\theta}_y + C_y\theta_y \end{cases} \tag{7}$$

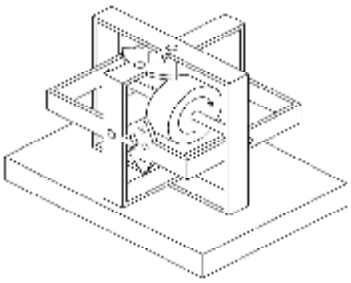

Figure 1 - A simplified illustration of a 2 DOF mechanical free gyro

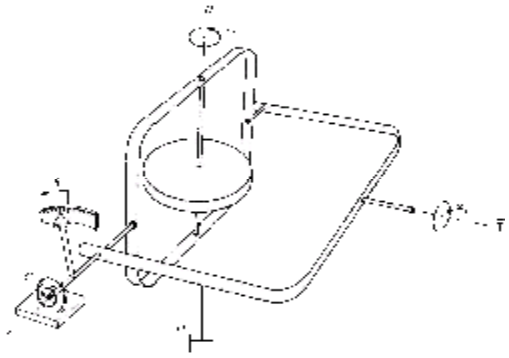

Figure 2 - Spring, damper and pickoff of a gimbal

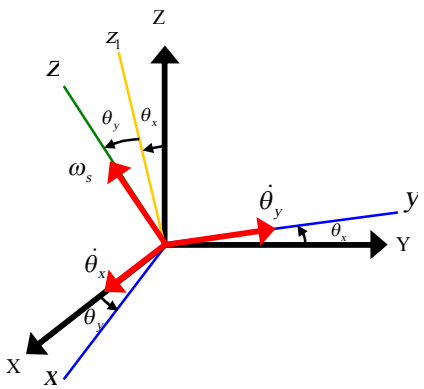

Figure 3 - The manner of arriving gimbals at final position

To obtain the state-space equation of the gyro, the following state variables are defined

$$\begin{cases} x_1 = \theta_x \\ x_2 = \theta_y \end{cases}, \quad \begin{cases} x_3 = \dot{\theta}_x \\ x_4 = \dot{\theta}_y \end{cases} \tag{8}$$

which lead to

$$\begin{cases} \dot{x}_1 = x_3 \\ \dot{x}_2 = x_4 \\ \dot{x}_3 = \dfrac{2I - I_z}{I} x_2 x_3 x_4 - \dfrac{H}{I} x_4 - \dfrac{D_x}{I} x - \dfrac{C_x}{I} x_1 + \dfrac{1}{I} T_x \\ \dot{x}_4 = -\dfrac{I - I_z}{I} x_2 x_3^2 + \dfrac{H}{I} x_3 - \dfrac{D_y}{I} x_4 - \dfrac{C_y}{I} x_2 + \dfrac{1}{I} T_y \end{cases} \tag{9}$$

Linearizing (9) about the zero equilibrium point yields the linear time-invariant model of the gyro. The state-space model of this linear system is equal to

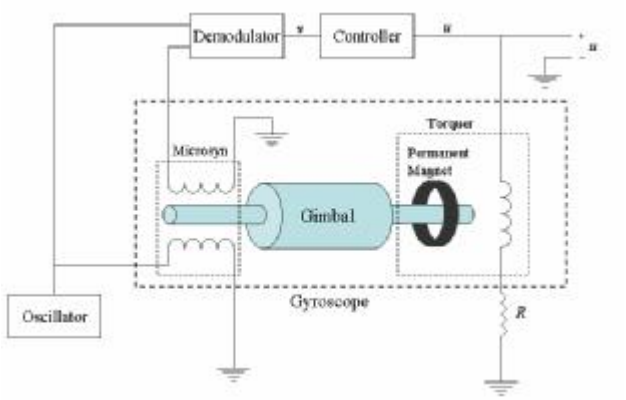

Figure 4 - Control structure of closed-loop system

Table 1: Nominal value of gyro parameters

Parameter	Description	Value
H	Rotor angular momentum (Kg.m^2/s)	0.075
D_x, D_y	Damping coefficients of two axis (Pa.s)	0.05
C_x, C_y	Spring constants of two axis (N/m.rad)	1
I	Gimbal moment of inertia (kg.m^2)	2.34x10^{-4}

$$\dot{X} = \begin{bmatrix} 0 & 0 & 1 & 0 \\ 0 & 0 & 0 & 1 \\ -\frac{C_x}{I} & 0 & -\frac{D_x}{I} & -\frac{H}{I} \\ 0 & -\frac{C_y}{I} & \frac{H}{I} & -\frac{D_y}{I} \end{bmatrix} X + \begin{bmatrix} 0 & 0 \\ 0 & 0 \\ \frac{1}{I} & 0 \\ 0 & \frac{1}{I} \end{bmatrix} \begin{bmatrix} T_x \\ T_y \end{bmatrix} \quad (10)$$

$$y = \begin{bmatrix} 1 & 0 & 0 & 0 \\ 0 & 1 & 0 & 0 \end{bmatrix} X$$

3. Control Structure of the System

The closed-loop system includes the gyroscope, the pick-off, the torquer, and the controller. A Microsyn with 0.01 degree of accuracy is used as the pick-off and a permanent magnet motor is employed as the torquer. Fig. 4 shows the control structure of the closed-loop system.

An oscillator is used to apply the AC signal to the primary coil of the microsyn and to the first input of the demodulator. The microsyn is arranged such that a rotational displacement in the output shaft produces an output signal in the secondary coil that is proportional to the amplitude and direction of the rotational displacement of the shaft; then, the produced signal is applied to the second input of the demodulator. The demodulator produces a relatively slowly varying displacement modulation signal *v*, which is the input to the controller [7]. Then, the control signal *u* is applied to the torquer, which results in producing the required torque in order to bring the gimbals to their equilibrium point.

Therefore, the control aim is to keep gimbals in their equilibrium point. In this case, the measurement angular rates of the vehicle can be obtained by multiplying the measured control signal by the system scale factor.

System Scale Factor

In this section, the scale factor of the closed-loop system is investigated. From the block diagram shown in Fig 5, the closed-loop gain is equal to $K_{cl} = k_t / H$, where k_t is the scale factor of the torquer. The transfer function of the torquer that is used in this structure is equal to

$$G_t = \frac{T_c}{u} = \frac{47.9915\ (s + 4.224)}{(s + 818.2)\,(s + 8.273)}, \quad (11)$$

where the numeric values are obtained from a typical 2DOF gimbal gyro. Hence, the scale factor of torquer is equal to:

$$k_t = 0.0299 \quad N.m/\,v \quad (12)$$

Finally, the measurement angular rates of the vehicle will be achieved using the following equation:

$$\omega = K_{cl} \times u \quad (13)$$

Table 1 shows the nominal values of the gyro parameters.

4. Nature of Faults Considered

Some of the most important error sources in gyros are spin motor, flex leads, ball bearings, mass imbalance, dampers, springs, pick-offs, and environments [6]. The sources of these errors are mostly: nonlinearity effects of the change in temperature on system parameters, unsuitable feeds, friction, and asymmetry. Among these, effects of the temperature change can cause serious errors. There are other sources of major errors such as gimbals reaction and nutation, which affect the transient response of the closed-loop system. The controller should remove these errors from the system response.

The following errors are considered in this paper:

(1) **Bias**: a constant offset between the input and output of the gyro

(2) **Drift**: a time-varying offset at the output of the gyro that can be characterized as:
- **Random drift**: random changes in the direction and/or the magnitude of the gyro error over time
- **Systematic drift**: can be modeled deterministically with the particular dynamics involved

(3) **Measurement noise**: an error due to measurements such as A/D or pick-off resolution (about 0.01°).

5. Simulation Results

In this paper, the LQG/LTR method [8] is employed to achieve the control goals. Fig. 5 shows the block diagram of the control structure, where

- e: input error torque
- w: disturbance torque involving drift and bias errors
- T_{in}: gyro input torque (due to vehicle movements)

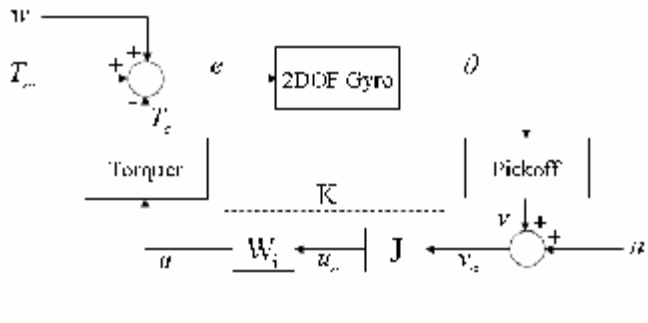

Figure 5 - Block diagram of closed-loop control structure

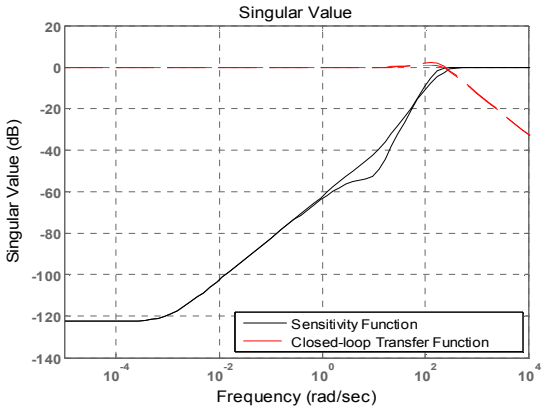

Figure 6 - Sensitivity (-) and closed-loop transfer (--) functions

- θ : gimbals position (should always be zero)
- n: measurement noise
- u: control signal
- T_c: control torque

The weighting function W_i is applied for the integral action and is equal to

$$W_i = \begin{bmatrix} \dfrac{1}{s+0.001} & 0 \\ 0 & \dfrac{1}{s+0.001} \end{bmatrix} \qquad (14)$$

The controller J consists of a Kalman Filter and an LQR controller. Because of the nature of these two parts, stability of the closed-loop system is guaranteed inherently. Thus, the control problem reduces to design a Kalman and an LQR gains. The state-space equations of the controller is

$$J : \begin{bmatrix} \dot{X}_j \\ u_n \end{bmatrix} = \left[\begin{array}{c|c} A - BK_c - K_f C & K_f \\ \hline -K_c & 0 \end{array}\right] \begin{bmatrix} X_j \\ v_n \end{bmatrix} \qquad (15)$$

where K_f and K_c are the Kalman and LQR gains, respectively, and A, B and C are the state-space matrices of the system, which consists of the gyro, the torquer, the pick-off and W_i. K_f and K_c should be designed such that all poles of the closed-loop system lay in the left half of the *s*-plane.

Fig. 6 shows the sensitivity (S) and the sensitivity complement (T) of the system. According to this figure, $\|T\|_\infty = 1.27$. Therefore, the closed-loop system should have good robustness behavior when it encounters parameter changes and disturbances. Fig. 7 shows measurement of angular rates, desired outputs and gimbals position of the nominal closed-loop system without any disturbance and measurement noise.

In order to show the behavior of the designed controller, four faults (given in Table 2) are examined. The simulation results are shown in Figs 8--10. As these figures show, the closed-loop system has good robustness against these faults. Therefore, the control requirement (i.e. fixing gimbals at the equilibrium position) is satisfied.

Bias and other similar changes in the parameters, which cause change in the scale factor, should be measured before starting the vehicle. If the scale factor changes while the vehicle is working, the output may contain errors. Therefore, bias and other similar changes in the scale factor should be measured and the standard deviation and the mean of changes should be updated daily. By using these parameters, the measurement accuracy can be increased during the system operation.

6. CONCLUSION

In this paper, dynamic equations and the control of the 2DOF gimbal gyro was considered. This proposed method can eliminate gimbal lock and some disturbances in such gyros and reduce the effects of some faults such as nutation, bias, drift, and measurement noises. The gimbals are held in their equilibrium position using an LQG/LTR controller which also stabilized the closed-loop system. The output measurement angular rate was achieved via the torquer input voltage multiplied by the system scale factor. Further works include improvement in the measurement accuracies and robustness of the closed-loop system against effects of changes in the temperature on system parameters and eliminating the nutation fault in such gyros.

REFERENCES

[1] H. Chingiz, and C. Fikret, "Sensor and control surface/actuator failure detection and isolation applied to F-16 flight dynamic," *Aircraft Engineering and Aerospace Technology*, vol. 77, no. 2, pp. 152-160, 2005.

[2] P.S. Maybeck, and R.D. Stevens, "Reconfigurable flight control via multiple model adaptive control methods," *IEEE Transactions on Aerospace and Electronic Systems*, vol. 27, no. 3, pp. 470-480, 1991.

[3] P.S. Maybeck, "Multiple model adaptive algorithms for detecting and compensating sensor and actuator/surface failures in aircraft flight control systems," *International Journal of Robust and Nonlinear Control*, vol. 9, no. 14, pp. 1051-1070, 1999.

[4] Y. Zhang and J. Jiang, "Integrated active fault-tolerant control using IMM approach," *IEEE Transaction on Aerospace and Electronic Systems*, vol. 37, no. 4, pp. 1221-1235, 2001.

[5] Y. Zhang and J. Jiang, "Modeling of rate gyroscopes with consideration of faults," *IFAC-Safe Process*, 168-173, 2006.

[6] M. D. Ardema, *Newton-Euler Dynamics*, Springer Science, New York, 2005.

[7] M. G. Koning, "Torquer scale factor temperature correction means," *United States Patent*, Appl. no. :384,246, 1975.

[8] J. M. Maciejowski, *Multivariable Feedback Design,* Addison-Wesley, Wokingham, England, 1989.

Table 2: most common faults

Case No.	Description of fault	Simulated fault value	Fault pattern
1	Constant Parasitic torque (N.m)	0.1746 (equal to 0.013 rad/s)	Bias
2	Random disturbance (N.m)	Standard deviation 0.01	Random drift
3	Time varying parasitic torque (N.m)	1° per 10 minutes	Systematic drift
4	Random measurement noise (volts)	Standard deviation 1.4×10^{-4} (equal to 0.01°)	Pick-off Measurement noise

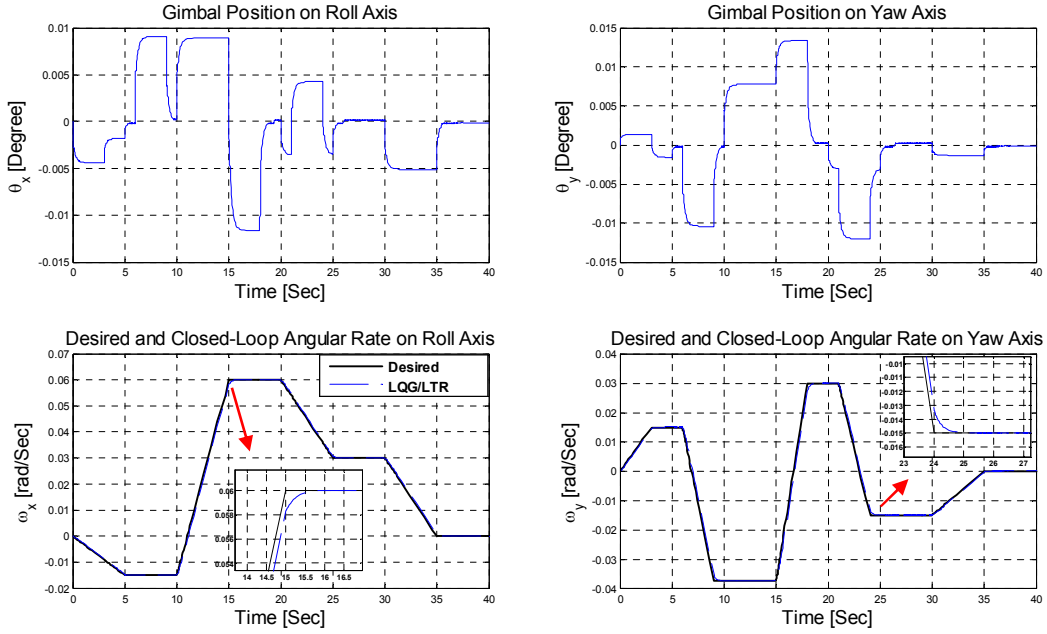

Figure 7 - Nominal response of 2DOF gyro including gimbal position, desired angle (−), measured angular rate (--)

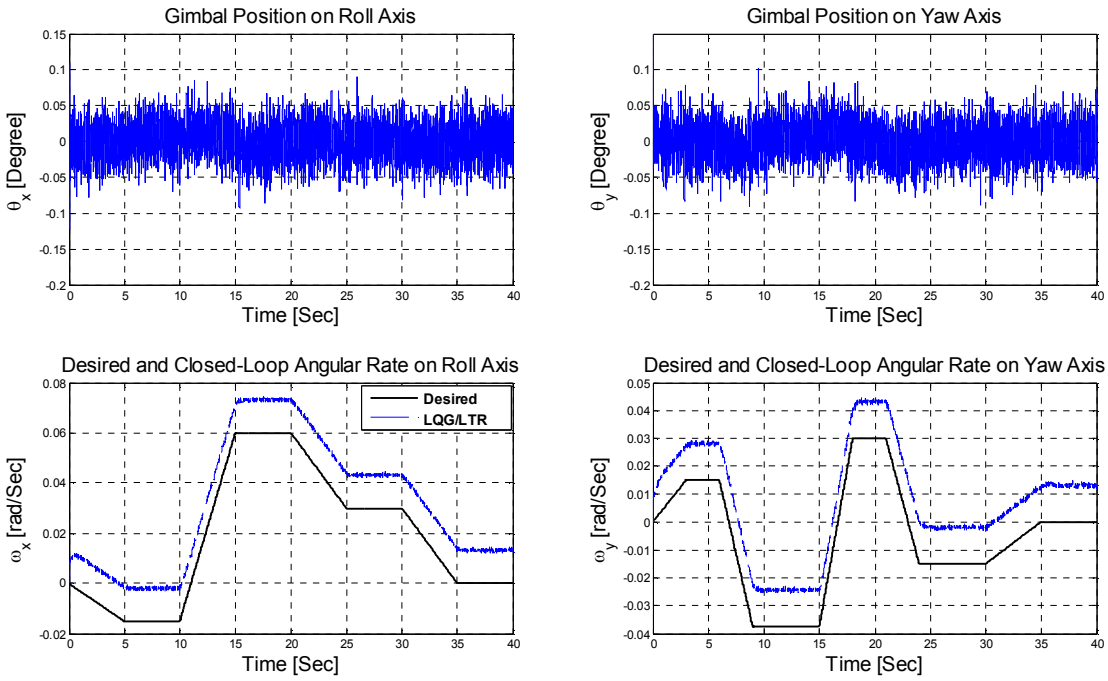

Figure 8 - Fault illustration under cases #1, #2 and #3 (bias, random and systematic drift)

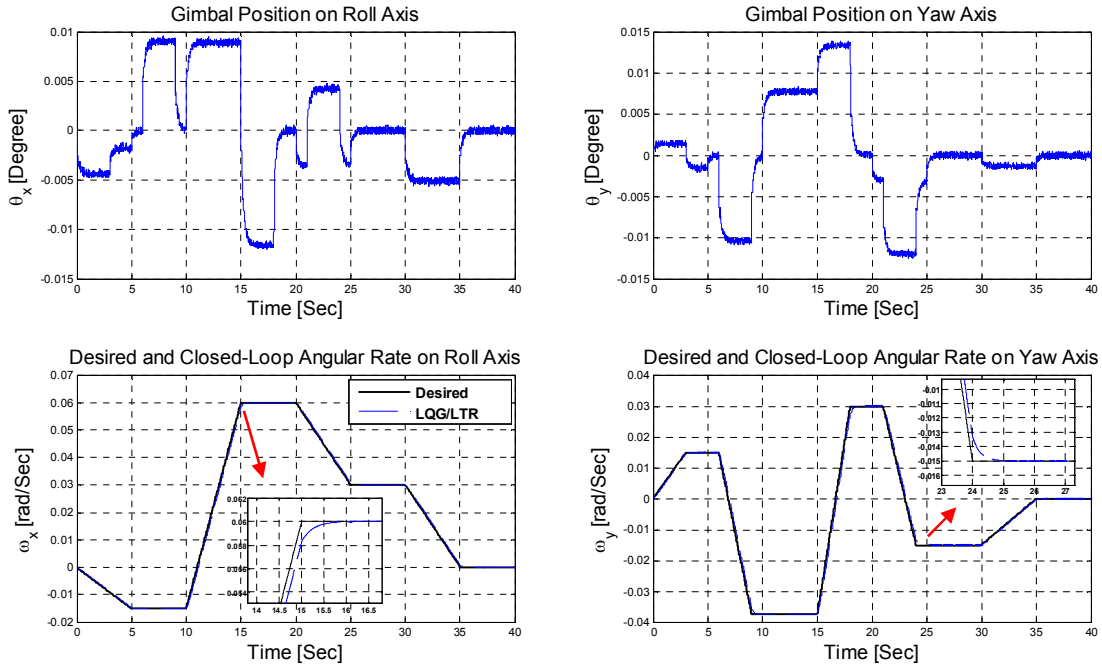

Figure 9 - Fault illustration under case #4 (measurement noise)

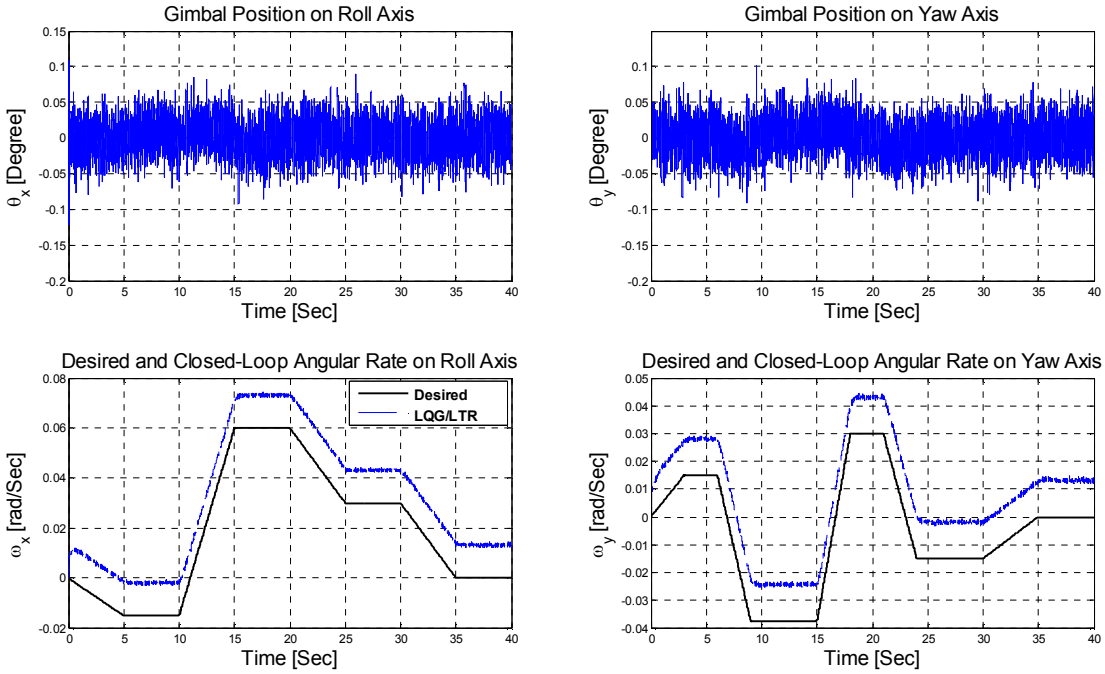

Figure 10 - Fault illustration under cases #1 to #5 (all patterns)